Acta Biomaterialia 128 (2021) 502–513

Contents lists available at ScienceDirect

Acta Biomaterialia

journal homepage: www.elsevier.com/locate/actbio

Full length article

Monetite-based composite cranial implants demonstrate long-term clinical volumetric balance by concomitant bone formation and degradation

Susanne Lewin[a,*], Lars Kihlström Burenstam Linder[b], Ulrik Birgersson[b,c,d], Sara Gallinetti[a,d], Jonas Åberg[a,d], Håkan Engqvist[a], Cecilia Persson[a], Caroline Öhman-Mägi[a]

[a] Department of Materials Science and Engineering, Uppsala University, Uppsala, Sweden
[b] Department of Neurosurgery, Clinical Neurosciences, Karolinska University Hospital and Karolinska Institutet, Stockholm, Sweden
[c] Department of Clinical Science, Intervention and Technology, Division of Imaging and Technology, Karolinska Institutet, Huddinge, Sweden
[d] OssDsign, Uppsala, Sweden

ARTICLE INFO

Article history:
Received 11 January 2021
Revised 1 April 2021
Accepted 7 April 2021
Available online 20 April 2021

Keywords:
Cranioplasty
Bioceramics
Calcium phosphate
Computed tomography
Quantitative analysis

ABSTRACT

The use of calcium phosphates (CaPs) as synthetic bone substitutes should ideally result in a volumetric balance with concomitant bone formation and degradation. Clinical data on such properties is nevertheless lacking, especially for monetite-based CaPs. However, a monetite-based composite implant has recently shown promising cranial reconstructions, with both CaP degradation and bone formation. In this study, the volumetric change at the implant site was quantified longitudinally by clinical computed tomography (CT).

The retrospective CT datasets had been acquired postoperatively ($n = 10$), in 1-year ($n = 9$) and 3-year ($n = 5$) follow-ups. In the 1-year follow-up, the total volumetric change at the implant site was -8 ± 8%. A volumetric increase (bone formation) was found in the implant–bone interface, and a volumetric decrease was observed in the central region (CaP degradation). In the subjects with 2- or 3-year follow-ups, the rate of volumetric decrease slowed down or plateaued. The reported degradation rate is lower than previous clinical studies on monetite, likely due to the presence of pyrophosphate in the monetite-based CaP-formulation. A 31-months retrieval specimen analysis demonstrated that parts of the CaP had been remodeled into bone. The CaP phase composition remained stable, with 6% transformation into hydroxyapatite. In conclusion, this study demonstrates successful bone-bonding between the CaP-material and the recipient bone, as well as a long-term volumetric balance in cranial defects repaired with the monetite-based composite implant, which motivates further clinical use. The developed methods could be used in future studies for correlating spatiotemporal information regarding bone regeneration and CaP degradation to e.g. patient demographics.

Statement of significance

In bone defect reconstructions, the use of calcium phosphate (CaP) bioceramics ideally results in a volumetric balance between bone formation and CaP degradation. Clinical data on the volumetric balance is nevertheless lacking, especially for monetite-based CaPs. Here, this concept is investigated for a composite cranial implant. The implant volumes were quantified from clinical CT-data: postoperatively, one year and three years postoperatively.

In total, -8 ± 8% ($n = 9$) volumetric change was observed after one year. But the change plateaued, with only 2% additional decrease at the 3-year follow-up ($n = 5$), indicating a lower CaP degradation rate. Osseointegration was seen at the bone–implant interface, with a 9 ± 7% volumetric change after one year. This study presented the first quantitative spatiotemporal CT analysis of monetite-based CaPs.

* Corresponding author at: Div. of Applied Materials Science, Dept. of Materials Science and Engineering Sciences, Uppsala University, Box 35, 751 03 Uppsala, Sweden.

E-mail address: susanne.lewin@angstrom.uu.se (S. Lewin).

https://doi.org/10.1016/j.actbio.2021.04.015

1. Introduction

Being inherently bioactive and osteoconductive, calcium phosphates (CaPs) are excellent synthetic bone substitutes [1]. Additionally, their biodegradability facilitates osteoconduction at the surface and inside the pores of the implant. The degradation occurs either passively by dissolution or actively by cell-mediated resorption, where the CaP phase directs the degradation rate. Ideally, bone formation and CaP degradation take place at a similar rate, resulting in volumetric balance and mechanical stability at the implant site [1].

Reconstruction of large cranial defects following neurosurgery or trauma remains a major clinical challenge [2]. Currently used reconstruction methods include either autologous bone or synthetic implants. The reported complication rate is high (∼20%) and infection is the most common complication [2,3]. As the most frequently used synthetic implant materials, e.g. PMMA or PEEK, are bioinert and lack osteoconductivity, the use of bioactive and osteoconductive materials could lead to improved clinical outcomes [4–7]. The clinically used bioactive implants are either calcium phosphate based implants [4,5,7], or fiber-reinforced bioglass composite implants [6,8,9]. Implants with osteoinductive factors (BMP-2) have also been used [10,11], but no wide-spread clinical use is seen for these implants so far. As for CaP-based implants, sintered hydroxyapatite (HA) have demonstrated both osteoconduction and bone-bonding[1] at the implant interface [5]. However, the biodegradability of HA is generally slower than bone formation [12]. Osteoconduction could possibly be improved by using CaP phases with a higher degradation rate, e.g. brushite or monetite [13]. Nevertheless, longitudinal studies on CaP degradation in patients are rare [14], especially for monetite [13]. Such data would be of high importance since the CaP degradation rate observed in patients is often different compared to that in animal models [14,15]. To the best of the authors' knowledge, only one study has quantified monetite degradation in patients. Tamimi et al. (2010) implanted monetite granules into alveolar bone defects of five patients [15]. After six months, the amount of regenerated bone (60%) and resorbed monetite (74%) was significantly higher compared to the control (bovine hydroxyapatite). The healing of large cranial defects requires more time than six months. A more suitable degradation rate seems to be obtained when monetite is combined with less soluble CaP phases, and implanted in blocks rather than granules [4].

This study focuses on a recently developed patient-specific calcium phosphate-titanium (CaP–Ti) cranial implant, which uses the above-mentioned monetite-based CaP [4,16–20]. The CaP formulation consists mainly of monetite (∼86%), with small fractions of β-tricalcium phosphate (∼8%; β-TCP) and β-calcium pyrophosphate (∼6%; β-CPP). The presence of β-CPP has been shown to slow down the degradation rate [17,21]. An additively manufactured titanium structure reinforces the implant, since CaP materials on their own have limited mechanical performance [22]. Promising outcomes have been observed in pre-clinical and clinical studies for this implant [4,16–20]. A recent retrospective study showed a particularly promising outcome [16]. The study evaluated a cohort of 50 subjects who previously had a 64% failure rate with autologous bone or other synthetic implants. In this complex cohort a total of 53 cranioplasties were performed using the CaP–Ti implant, of which only 7.5% subsequently developed complications that led to implant removal. Most of the removals were related to wound dehiscence in patients with thin and fragile soft tissue [16]. In retrieval implants, bone formation has been demonstrated in four patients [16,17,19]. Nevertheless, the increased and successful clinical use of the implant has sparked an interest for more detailed knowledge of the longitudinal degradation and bone regeneration capacity of this specific CaP formulation in patients.

Computed tomography (CT) is the standard imaging method for clinical follow-up of cranial reconstruction. Hence, these images could be evaluated retrospectively in further analyses. Quantitative analysis of CT images involves the calculation of specific parameters, such as volume and density [23]. Hounsfield units (HU) are commonly used to describe the X-ray attenuation in CT images and relate this to density [24]. In the field of cranioplasty, to the best of the authors' knowledge, only three studies have applied image analysis techniques to systematically evaluate autologous bone resorption in CT images [25–27]. Quantitative CT evaluation of bone formation in HA cranial implants have been attempted only in three previous studies [27–29]. In two of these studies, the analysis was restricted to qualitative scoring of the degree of bone-bonding at the implant interface and evaluation of HU [27,28]. Qualitative scoring comes with inherent limitations of subjectivity. One previous study used image analysis for volumetric quantification of sintered HA implants [29]. The study provided interesting results, where bone-bonding at the interface could be objectively measured. However, this and the previously mentioned studies compared isolated time-points [27–29]. The image analysis methods could be further developed by using techniques applied in other longitudinal imaging studies [30], such as image registration, i.e. by superimposing scans from different time-points.

The aim of this study was to conduct longitudinal volumetric investigations on the CaP–Ti implant under clinical conditions. In addition, a retrieval specimen from one of the subjects was available and analyzed in more detail. The hypothesis was that the volume at the implant site is maintained through a balance between bone formation and CaP degradation. Overall, the study makes methodological advancements on clinical evaluations of CaPs by spatiotemporal quantitative analysis of clinical CT images. The study furthermore demonstrates successful bone-bonding and long-term volumetric balance in the clinical use of the CaP–Ti cranial implant, and reports longitudinal volumetric clinical data for a monetite-based CaP.

2. Materials and methods

2.1. Subjects and clinical procedures

This retrospective study included a subset of subjects from a larger cohort in a previous study [16]. Subjects eligible for the study had undergone cranioplasty with a CaP–Ti implant (OssDsign Cranial PSI, OssDsign AB, Uppsala, Sweden) following an open cranial defect, from November 2014 until June 2016 at the Department of Neurosurgery, or at the Plastic Surgery Section (Karolinska University Hospital, Stockholm, Sweden). Subjects who did not have at least one postoperative (baseline) and one follow-up CT scan were excluded from the study. Subjects were excluded if the CaP-Ti implants had been placed either in combination with another implant or in small defects (< 25 cm^2). Furthermore, in order to verify the scan quality between time-points, an additional exclusion criterion based on similarity between the scans in a control region was applied (further described in Section 2.2.3).

The manufacturing of the implants (OssDsign Cranial, OssDsign, Uppsala, Sweden) has been described previously [4]. In short, the implants are designed based on the patients CT-images. The titanium mesh-type structures (∼1.8 mm thickness) are then additively manufactured in Ti-6Al-4 V. CaP is molded around the implant in hexagonally shaped tiles (∼6 mm thickness). Fixation arms are incorporated in the titanium structures. During surgery, these

[1] In this study, the term bone-bonding describes contact between the implant and the recipient bone, similar to the term osseointegration – more frequently used for intact implants (e.g. metal implants).

are used when inserting screws for fixation into the cranial bone of the patient.

Approval from the institutional review board was given by the regional ethics committee at Karolinska University hospital, Stockholm (Dnr 2017/251031). The patient with the retrieval specimen provided signed informed consent. All the postoperative CT-scans were part of the clinical follow-up regimen.

2.2. Quantitative analysis of clinical CT images

The CT images were obtained as DICOM-files. The metadata of the scanning parameters was collated from each scan. Subsequently, image processing and image analysis were completed in 3D slicer (http://www.slicer.org) [31]. An overview of the image processing workflow is presented in Fig. 1. Each analysis step is briefly presented below, more details are given in the supplementary material (S1).

2.2.1. Registration

For the same subject, the baseline and follow-up images were superimposed by rigid registration. The registration aligned scans from the different time-points. After registration, all scans from the same patient had common coordinates, which later ensured that the quantifications were conducted in the same implant regions across all time-points. Further information about the registration parameters can be found in the supplementary material (S1).

2.2.2. Segmentation

A semiautomatic segmentation process was performed in order to separate the bone and implant from the surrounding soft tissue. Bone and CaP had to be segmented together since these phases were not possible to separate due to their similar X-ray attenuation and the limited resolution of the clinical CT images. The full implant was included in the segmentation (and later in the quantitative measurements), i.e. all hexagonal calcium phosphate tiles and the titanium structure (Fig. 1). The segmentation was conducted using a global threshold based on the Otsu method [32]. To remove noise, only segmented clusters above 5 voxels were included. Further details and an analysis of the sensitivity of the thresholding process can be found in the supplementary material (S1).

2.2.3. Quantification in the control region

For each subject, part of the cranial bone was used as control for the image processing (Fig. 1). The bone volume was quantified in the same circular control region ($\varnothing = 80$ mm) across all time-points for each subject, the region of interest (ROI) was referred to as $ROI_{control}$. In this region, the bone remodeling should be stable. Hence, no volumetric changes were expected between baseline and the follow-ups. The absolute volumetric difference in the control region, between baseline and each follow-up, was calculated for each subject. Subjects with an absolute volumetric change above 3% across time-points were excluded from further analysis due to the possibly low quality of the CT scans. A variation of 3% has been found for non-changing objects in clinical images in a previous study [33], and similar numbers have also been suggested in another study [25]. It was accordingly set as the lowest detectable volumetric difference. In addition, the Dice similarity coefficient (DSC) and Hausdorff distance (HD) were calculated in the control region between time-points to measure the overlap [34,35]. The DSC measures the spatial overlap, from zero to one, where one equals full overlap. HD is the greatest distance from a point in one volume to the closest point in the other volume.

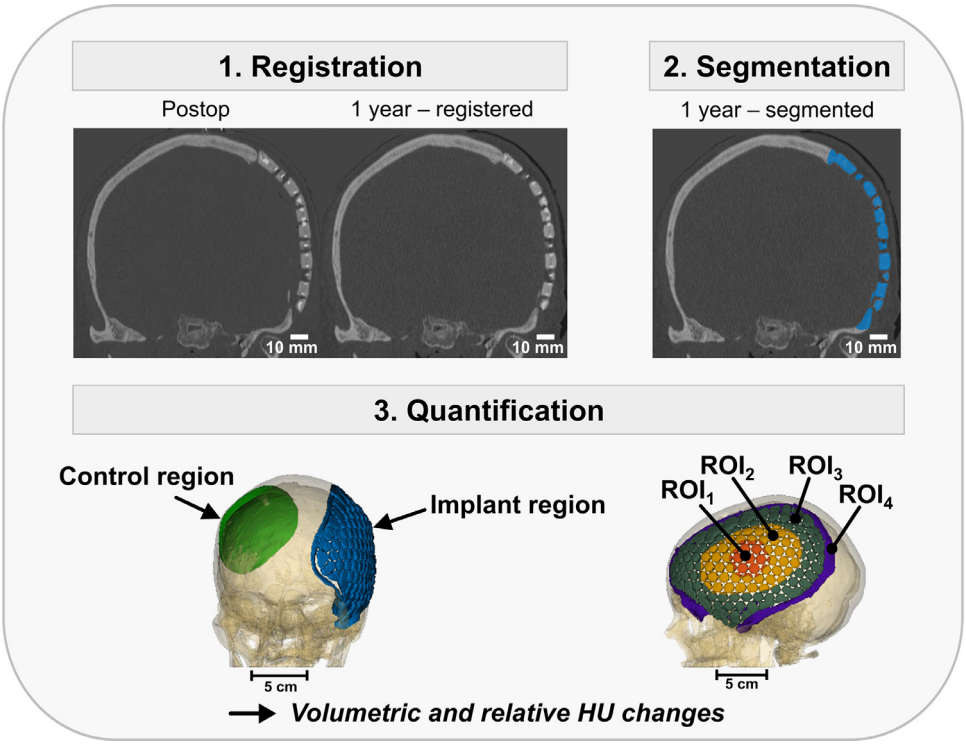

Fig. 1. An overview of the different image processing steps in the workflow. **Registration:** CT images in the coronal plane for one subject. The images are from the postoperative CT, and the 1-year follow-up after registration. **Segmentation:** CT image from the same 1-year follow-up, where the implant region has been segmented (blue). **Quantification:** The regions used in the quantification are indicated in 3D rendered models of the segmented volume. The implant region (i.e. the implant and the bone defect edge, $ROI_{implant}$) and the control region ($ROI_{control}$) are visualized in blue and green, respectively (left). The different regions of interest (ROIs) are visualized in different colors (right); ROI_1 (orange), ROI_2 (yellow), ROI_3 (green), and ROI_4 (purple).

2.2.4. Quantifications in the implant region

The ROIs of the implant were created semi-automatically (for details, see supplementary material S1). In brief, a ROI covering the bone defect edge and implant was created based on the titanium structure referred to as $ROI_{implant}$ (Fig. 1). Four additional ROIs were created in order to quantify changes in different locations of the implant. ROI_1 was created around seven tiles selected in the middle of each implant. ROI_2 and ROI_3 were created on the remaining part of the implant, in the same shape as the outline of the implant and divided by half the distance to the implant edge. The remaining region, ROI_4, corresponded to the interface between the implant and the bone defect edge. The regions can be observed in Fig. 1. The segmented volume was quantified for each time-point in each of the following regions: $ROI_{control}$, $ROI_{implant}$, ROI_1, ROI_2, ROI_3, and ROI_4. The volumetric differences between the baseline scan and the later time-points were calculated for each subject.

A distance map of $ROI_{implant}$ was created for each subject to visually observe the volumetric changes. The distance maps compare the distances between the follow-up and the baseline volumes in the implant region. The changes observed in the distance maps were also compared visually to the CT images. The implant size of each implant was calculated based on the titanium structure. Subsequently, the subjects could be divided into two size groups: $< 100\ cm^2$ and $\geq 100\ cm^2$.

2.2.5. Relative density in the implant region

Since no phantom (with controlled density) was included during the CT-scans in this study, the HU-values were not calibrated for densities close to bone and CaP material. The HU-values could therefore vary between time-points due to e.g. small differences in scanning protocols [36,37]. The use of intra-patient calibration of HU-values has been shown to improve the reliability in such datasets [25,38]. Therefore, an average HU-value was calculated in the segmented control regions ($HU_{control}$). This value was then used for an intrasubject calibration of relative HU-values for each CT-scan.

To estimate changes in density for each region ($ROI_{implant}$, ROI_1, ROI_2, ROI_3, and ROI_4) between time-points, mean HU-values were obtained from the respective segmented regions for each follow-up. The mean HU-values were calculated in the volume segmented in the last follow-up i.e. the 1-year follow-up for most subjects. Subsequently, an intrasubject calibration of the obtained HU-values was conducted by dividing the mean HU-value for each scan by the $HU_{control}$ for the same scan. The change in relative HU-value was reported for each subject between baseline and follow-ups.

2.3. CaP material characterization and analysis of a retrieval specimen

2.3.1. The retrieval specimen

One subject underwent tumor resection of an osseous sphenoidal wing meningioma and was reconstructed with a CaP–Ti implant. In the clinical CT quantifications, the affected parts of the implant were excluded. The implant was removed thirty-one months later due to tumor regrowth in the orbit, which required surgery [16]. The retrieved specimen was fixated in formalin and embedded in PMMA. The embedded specimen was sectioned, and the histology sections were stained with paragon. The histology results have been reported previously [16], but are included in this study together with more detailed analysis of the material. Additionally, the remaining intact parts of the specimen were analyzed by micro-computed tomography (µCT) – desktop and synchrotron-based – following histology sectioning. Again, parts of the implant affected by the meningioma were excluded.

The desktop µCT (SkyScan1172, Bruker Corp., Belgium) was performed at 100 kV and 100 µA, with a Cu-Al filter. An isotropic pixel size of 5.4 μm was used. Cross sections were reconstructed using NRecon (NRecon 1.7.1.0, Bruker Corp., Belgium). Following the analysis of the desktop µCT images, three parts of the retrieval specimen were selected to be analyzed by synchrotron radiation phase contrast µCT (SR-µCT). The SR-µCT was performed at the TOMCAT beamline (Paul Scherrer Institute (PSI), Switzerland) at a 3.25 μm isotropic voxel size with a phase-contrast method [39,40]. The beam energy during the scanning was 30 keV, and the ring current 400 mA. The images from the SR-µCT were reconstructed in ImageJ using a plug-in [41,42].

To identify any changes in the CaP material after 31 months in vivo, two control tiles of CaP-material were analyzed. The control tiles originated from the same batch as the CaP tiles in the retrieval specimen and had been stored for quality control in sterilization bags for 31 months at room temperature. These tiles were scanned at the TOMCAT beamline (Paul Scherrer Institute, Switzerland). Both the scanning and the reconstruction of the images were performed with the same settings as for the retrieval specimen. All image processing of µCT images was conducted in CTAn (CTAn 1.16.4.1, Bruker Corp., Belgium).

2.3.2. Validation of clinical CT results with desktop µCT

The reconstructed images from the desktop µCT were segmented by an automatic global threshold, based on the Otsu method. The parts of the retrieval specimen were visualized in 3D and compared to the clinical CT. On cross-sectional images from both imaging modalities, linear 2D measurements were made to determine the thickness of 10 different tiles.

2.3.3. Porosity analysis of CaP and retrieval specimen

In the SR-µCT datasets of the retrieval specimen, a ROI ($2 \times 4 \times 3$ mm) was created in the middle of five different tiles, in between the titanium structure. A ROI of the same size was also created in the CaP tiles that had been stored on the shelf for 31 months. Following an automatic global threshold based on the Otsu method, the porosity and pore size distribution were calculated.

2.3.4. Verification of bone formation in CT images through SR-µCT and histology

The SR-µCT datasets of the retrieval specimen were further analyzed and compared to the histology sections in order to identify regenerated bone. Moreover, a 3D visualization of the bone and the remaining CaP material was performed. All image processing was made in CTAn. In the segmentation process, the identification of bone and CaP was made using the histology and a previously developed method [43].

2.3.5. Phase composition

During the tumor resection surgery, loose fragments of the implant were collected and subsequently ground into a fine powder for phase characterization. Two additional powders, prepared from CaP tiles that initially came from the same batch as the CaP tiles in the retrieval specimen, were characterized: pre-implantation and stored 31 months on the shelf in sterilization bags at room temperature. The phase characterizations were performed by X-ray diffraction (XRD; D8 Advance, Bruker, AXS GmbH, Karlsruhe, Germany) using Ni-filtered Cu-Kα irradiation in a theta-theta setup with scanning diffraction angles (2θ) 4–70° in steps of 0.02° with 0.25 s per step, and a rotation speed of 80 rpm. In the pre-implantation sample, the scanning diffraction angles were 20–46° The phase compositions were quantitatively evaluated by Rietveld refinement (http://www.bgmn.de) [44] with a graphical user interface (http://www.profex.doebelin.org) [45]. Crystalline references used in the refinement were PDF #04–008–8714 for β-TCP [46],

PDF #04–013–3344 for brushite [47], PDF #04–009–3876 for β-CPP [48], PDF #04–009–3755 for monetite [49], PDF #01–074–0565 for HA [50] and PDF #04–013–3883 for octacalcium phosphate (OCP) [51]. No other phases were identified in the diffraction patterns.

2.4. Statistical analysis

Statistical analysis was performed in R (version 3.5.2) [52]. A paired *t*-test was performed in order to assess differences between volumetric change in the control and the implant region.

3. Results

3.1. Subjects and clinical procedures

Complete CT-datasets were available for 12 out of 31 eligible subjects. Two subjects were excluded due to a substantial volumetric change (above 3% between time-points) in the control region from the postoperative CT to the 1-year follow-up. Based on this criteria, three later follow-up CTs from the ten included subjects were also excluded. The included postoperative and 1-year postoperative datasets had the following acquisition parameters: the same scanner (Discovery CT750 HD, GE Healthcare, Wisconsin, USA), at 100 or 120 kVp, with a pixel spacing of 0.4 mm, a slice thickness off 0.625 mm or 1.25 mm, and reconstructed with the same convolution kernel (Boneplus). For the included subjects, the baseline CT had been performed between zero and five days postoperatively. The first follow-up was performed around one year postoperatively, between 285 and 462 days. In five subjects, additional CT datasets from roughly 3-years postoperative follow-ups (between 940 and 1173 days) were included. One subject only had a 2-year follow-up. The spread in acquisition parameters were larger for the later follow-ups: scanning at 100 or 120 kVp, with a pixel spacing of 0.4 mm, and a slice thickness off 0.8 mm, 0.625 mm or 1.25 mm. Three scanners had been used: Discovery CT750 HD (GE Healthcare, Wisconsin, USA), IQon Spectral CT (Philips Healthcare, Best, the Netherlands) and Aquilion ONE (Toshiba Medical Systems, Otawara, Japan). All images were reconstructed with bone convolution kernels (Boneplus-GE, YC-Philips and FC30-Toshiba).

The time-points for all CT-scans, and the age, sex and implant area of all subjects are presented in Table 1. The mean age of the subjects was 48 ± 18 years, and five males and five females were included.

3.2. Quantitative analysis of clinical CT images

The longitudinal volumetric differences are shown in Fig. 2. The mean absolute volumetric difference between all time-points was $0.8 \pm 0.5\%$ in $ROI_{control}$. An overlap of the segmented volumes in $ROI_{control}$ was demonstrated by the DSC being close to one (0.97 ± 0.01) and by the low HD (0.14 ± 0.04 mm). In $ROI_{implant}$, the mean absolute volumetric difference was $12 \pm 5\%$. The absolute mean volumetric differences in $ROI_{control}$ and $ROI_{implant}$ were significantly different ($p = 0.004$). A decrease in volume was seen in 7 out of 9 subjects at the 1-year follow-up in $ROI_{implant}$, with a mean volumetric change of $-8 \pm 8\%$. For the two subjects with an increase in volume, both implant sizes were below 100 cm^2. In the 2- or 3-year follow up ($n = 6$), the total mean volumetric change was $-10 \pm 13\%$, only a 2% additional change since the 1-year follow up. The volumetric difference ranged from −23% in a 3 year and 3 months follow-up (implant size > 100 cm^3), to 13% in a 2 year and 7 months follow-up (implant size < 100 cm^3). The mean relative HU change in $ROI_{implant}$ was $7 \pm 4\%$ in the 1-year follow-up, with an increase in eight out of nine subjects.

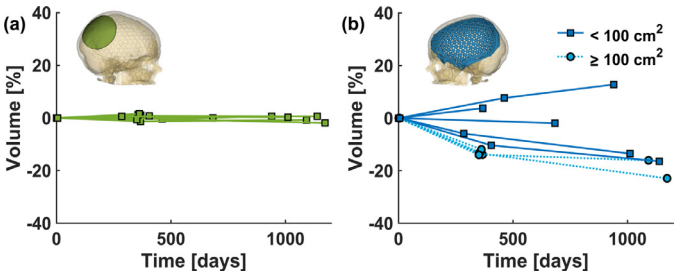

Fig. 2. Volumetric change vs. time for the control region **(a)** and the implant region (**b**).

Overall, the implants remained in place and the registration allowed for a detailed subject specific observation (Fig. 3). New bone formation and CaP degradation could be observed in all subjects. In general, the loss in volume of the CaP material mainly took place at the outer part of the implant, towards the scalp. Bone-bonding, defined as contact between the CaP-tiles and the recipient bone, was observed in large parts of the bone–implant interface (a quantification of the bone-bonding frequency can be found in the supplementary material S1). As expected, full bridging was more commonly seen at the later follow-ups. The full bridging was more frequently seen in cases where the implant had been placed closer to the bone defect edge (Fig. 3).

The longitudinal quantifications in the different implant regions can be seen in Fig. 4. In the central region of the implant (ROI_1), all subjects had a volumetric decrease (Fig. 4a). The mean volumetric change in the 1-year follow-up was $-14 \pm 8\%$ for the small implant group (< 100 cm^2), and $-18 \pm 2\%$ for the large implant group (≥ 100 cm^2). In the subjects with a 2 and 3-year follow-up, the change tended to decrease or plateau. In the five subjects

Table 1
Summary of the different CT scans. The age, sex and implant area for each subject. In addition, the number of days and volumetric difference ($ROI_{implant}$) postoperatively are presented for all subjects.

	Age	Sex	Implant area [cm^2]	CT 1 days	CT 2 days	CT 3 days	CT 1 volume	CT 2 volume	CT 3 volume
Subject 1	30	F	25	0	462	940	0%	8%	13%
Subject 2	70	F	75	1	–	683	0%	–	−2%
Subject 3	59	F	117	3	367	1092	0%	−14%	−16%
Subject 4	51	F	47	0	368	–	0%	4%	–
Subject 5	66	M	106	1	351	1173	0%	−13%	−23%
Subject 6	18	M	41	2	405	1139	0%	−10%	−16%
Subject 7	24	M	129	5	356	–	0%	−13%	–
Subject 8	41	M	205	2	362	–	0%	−12%	–
Subject 9	64	F	121	1	351	–	0%	−14%	–
Subject 10	48	M	76	5	285	1011	0%	−6%	−14%

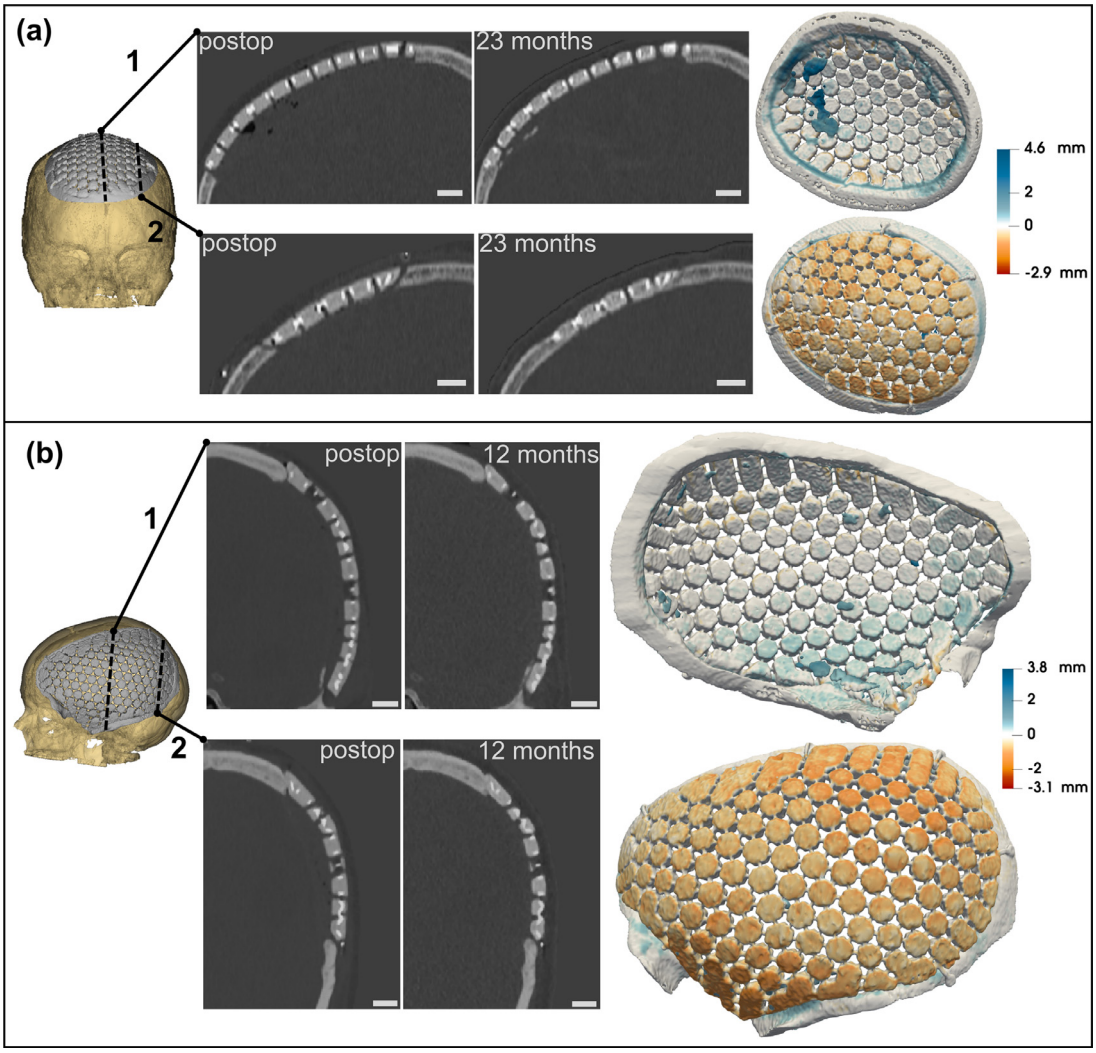

Fig. 3. Visualization of longitudinal follow-ups for two subjects. A 3D overview of the implants with two indicated sections across the implants (left). For these sections, the postoperative and last follow-up CT images are shown (scalebar = 10 mm). The difference in volumes are compared in 3D distance maps of the full implants (right). Volumetric increase is shown in blue, decrease in orange and the neutral regions (change within one voxel) in white. (a) CT images at both section 1 and 2 show full bridging and bone-bonding at the implant interface. (b) Full bridging is seen at the superior side of the bone–implant interface. At the inferior side, no bridging has occurred at section 2. For both subjects the CaP tiles have lost volume, mainly observed at the outer part of the implant.

with a 3-year follow-up, the volumetric change between the postoperative and the 1-year follow-up was -16 ± 6%, but the change at the later follow-up only had 6 ± 6% additional difference (in total -22 ± 9%).

In ROI_2 and ROI_3, the results were similar for all subjects (Fig. 4c and 4e). In both ROI_2 and ROI_3, at the 1-year follow-up, there was less mean volumetric change in the smaller implant group (-8 ± 6% and -6 ± 11%) than in the larger implant group (-16 ± 1% and -18 ± 3%). Volumetric decreases were observed in all except for two subjects (implant sizes < 100 cm^2), which had an increase in volume in ROI_3 (Fig. 4e) at the 1- and 3-years follow-up. In the region covering the bone–implant interface (ROI_4), no overall volumetric loss was observed (Fig. 4g). Instead a total volumetric increase was observed in all subjects (9 ± 7%). In the 1-year follow-up, the volumetric change was 13 ± 11% and 6 ± 1% for the small and large implant group, respectively. In the five subjects with 3-year follow-ups, the volume change from the postoperative CT to the 1-year follow-up was 9 ± 10%, and the change from the postoperative CT to the 3-year follow-up was in total 12 ± 13%.

The relative HU change in the 1-year follow-up increased in seven out of nine subjects in ROI_1 (2 ± 6%) (Fig. 4b). The relative change in ROI_2 (5 ± 3%) and ROI_3 (5 ± 5%), was higher in all subjects (Fig. 4d and 4f) regardless of implant size. In ROI_4, the relative HU change was 11 ± 5% (Fig. 4h) in the 1-year follow-up. In the subjects with longer follow-ups, the relative change in HU-value increased or plateaued in all regions.

3.3. CaP material characterization and analysis of a retrieval specimen

3.3.1. Validation of clinical CT with desktop μCT

The parts of the retrieval specimen were obtained following histology sectioning. Comparison of the desktop-μCT and to the last follow-up clinical CT for the same subject allowed for identification of the location of each part (Fig. 5a-d). Nevertheless, it was observed that damage had been caused at the removal of the implant and during the histological sectioning. The desktop μCT images were therefore used for identifying less damaged parts, which

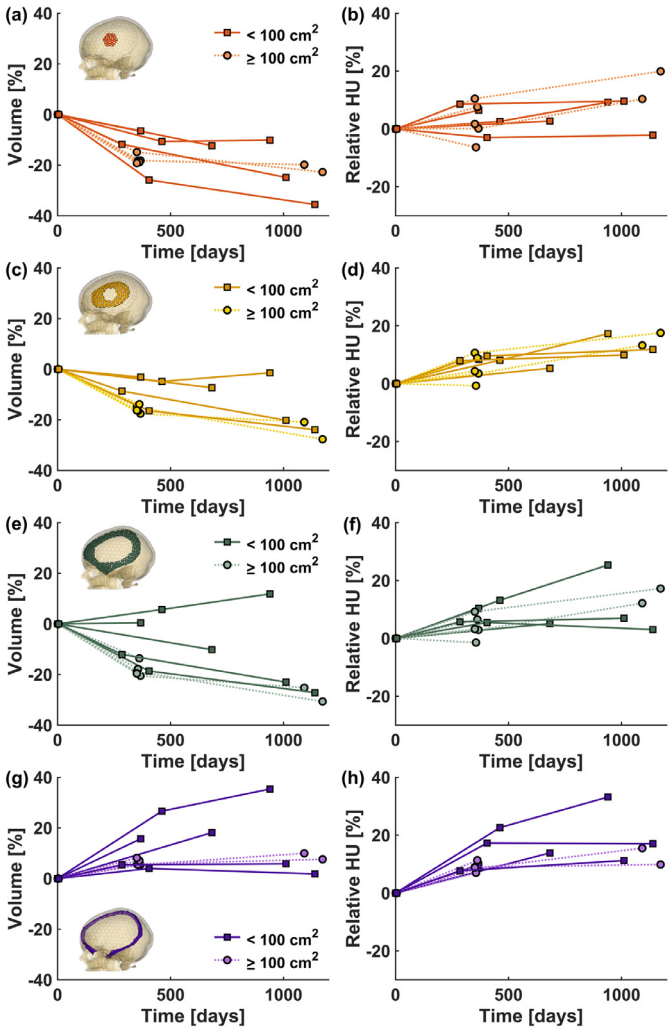

Fig. 4. Quantitative longitudinal changes in the different implant regions. The volumetric change (left) and relative HU change (right) vs. time for the different ROIs: ROI_1 (a-b), ROI_2 (c-d), ROI_3 (e-f) and ROI_4 (g-h). The implant sizes are marked by solid (< 100 cm^2) or dashed lines (≥ 100 cm^2).

were used in the SR-μCT analysis. The comparison between the measured tile thickness in the desktop μCT was 5.7 ± 0.5 mm vs. the clinical CT 5.8 ± 0.6 mm.

3.3.2. Porosity analysis of CaP and retrieval specimen

The parts of the retrieval specimen analyzed by SR-μCT are marked in red in Fig. 5b. The difference between the desktop μCT and the SR-μCT images can be appreciated in Fig. 5d-e. Newly formed bone, as well as CaP resorption was observed in all scanned parts of the specimens.

The CaP tiles stored on the shelf had a lower porosity, 12% ($n = 2$), than the tiles from the retrieval specimen, which ranged from 14 to 19% ($n = 5$). It was observed that the pores in the retrieval specimen were larger than in the CaP stored on the shelf. Measurements of the pore size distribution confirmed these observations. Compared to the CaP stored on the shelf, the pore volume of the retrieval specimen had both an increased microporosity (< 100 μm) and an increased size of the larger pores (Fig. 6). The range of the largest pore were 416 – 501 μm in the retrieval specimen, and 254 – 267 μm in the CaP material stored on the shelf.

3.3.3. Bone formation in SR-μCT and histology

The histology presented in Fig. 7a confirmed the presence of newly formed bone in direct contact with the CaP. A SR-μCT image of a part of the implant was compared to a closely neighboring histological cross-section (Fig. 7b). The locations of newly formed bone in the SR-μCT images could be confirmed by histology. The same region of the implant is shown in an SR-μCT image from the top-view. Based on the histology, a threshold to separate the bone from the CaP in the SR-μCT dataset could be determined. A 3D-model of the bone formation around and within the CaP tiles is presented in Fig. 7c.

3.3.4. Phase composition

The phase compositions obtained from the XRD analysis and Rietveld refinement are presented in Fig. 8a. Prior to implantation, the phase composition consisted of monetite (85%), β-TCP (9%) and β-CPP (6%). After 31 months on the shelf, the CaP phase composition was similar: monetite (85%), β-TCP (9%) and β-CPP (5%), but also HA (1%). The material analyzed after 31 months in vivo had a larger amount of HA (6%) and also octacalcium phosphate (OCP; 2%). The dominating phase was still monetite (72%), followed by β-TCP (14%) and β-CPP (6%). One representative XRD-pattern for each specimen is presented in Fig. 8b, together with reference patterns for the identified phases.

4. Discussion

The overall aim of this study was to investigate the volumetric balance of the CaP–Ti implants under clinical conditions. More specifically, it aimed to longitudinally quantify and compare the bone and implant volume in CT images from ten subjects after cranial reconstruction. The quantitative image analysis revealed an initial overall decrease in CaP tile volume during the first year postoperatively, although a volumetric increase was found at the bone defect–implant interface in all subjects. At the longer follow-ups this decrease had slowed down or plateaued. The dominating mechanisms for the volumetric changes were bone formation and CaP degradation. An increase in relative HU values was observed in 9 out of 10 subjects over time in the implant region, indicating an increase in apparent density due to bone formation. Investigations of a 31-months retrieval specimen demonstrated concomitant bone formation and CaP degradation by histology and μCT analysis, and allowed for phase composition XRD-analysis.

A limited number of previous studies on sintered HA implants, have performed CT evaluations by combining quantitative methods and qualitative scoring [27–29]. Moles et al. (2018) found no sign of bone-bonding in 51% of the subjects ($n = 37$) in 2-year follow-ups [27]. Maenhoudt et al. (2018) reported quantitative CT evaluations in follow-ups on average 39 months postoperatively: in 29% no sign of bone-bonding was observed ($n = 17$). Nevertheless, in one third of the subjects bone-bonding was deemed higher than 50% [29]. In contrast, a study of six children (mean age 9.6 years) observed bone-bonding in all subjects [28]. Although bone-bonding seems to be limited in adult patients, sintered HA implants have shown positive clinical outcomes [5]. Further bone ingrowth would stabilize CaP implants mechanically and lead to increased vascularization in the defect region, which in turn could decrease the infection rate [53]. All subjects in the present study, independent of age, showed bone formation at the bone–implant interface in the 1-year follow-up. In six out of ten subjects, more than 50% bone-bonding was observed at the implant interface (see measurements on bone-bonding frequency in the supplementary material S1). However, a loss in volume was seen for the CaP tiles especially in the central part of the implant. Nevertheless, at the later time-points ($n = 6$) the CaP degradation rate had decreased or plateaued.

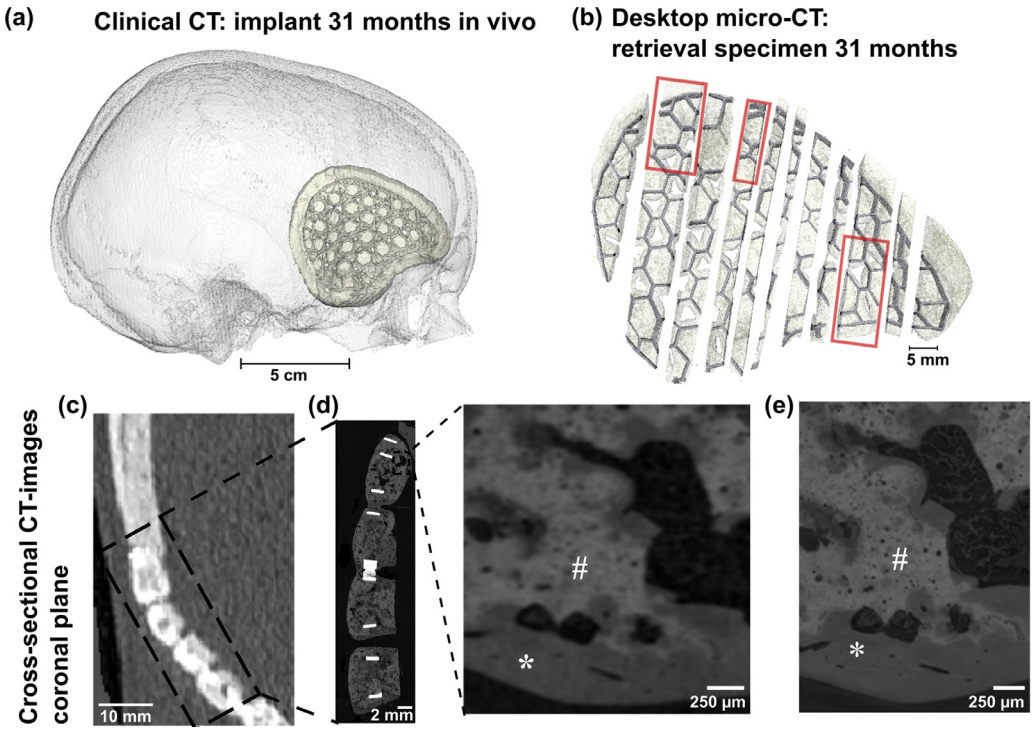

Fig. 5. Overview of the data for the subject from which the retrieval specimen was obtained. The clinical CT data is shown as a 3D rendered overview of the skull, with the location of the implant visible (a). A 3D rendering of the different parts of the retrieval specimen (b) reconstructed from the desktop µCT images, with the parts that were analyzed with SR-µCT marked in red. Coronal cross-sectional CT images from the clinical CT (c) and the desktop µCT (d). A region around a large pore is magnified (d), the same region is shown from a SR-µCT image (e). The lighter gray regions in (d) and (e) are the CaP material (#), the darker regions are newly formed bone (*).

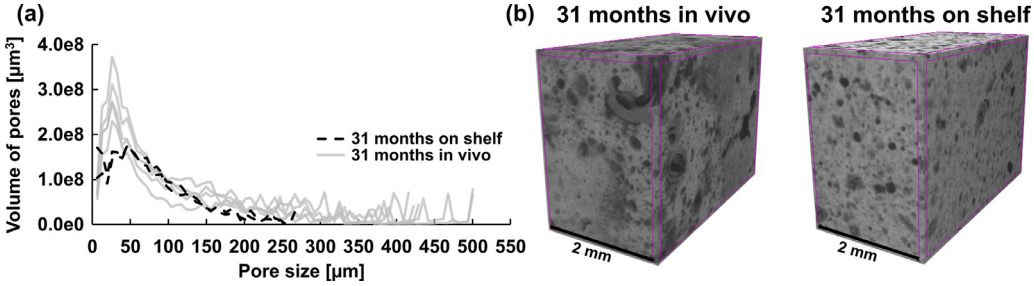

Fig. 6. Pore size distribution from the SR-µCT images from the CaP stored 31 months (black dashed lines) and from the 31 months retrieval specimen (gray solid lines) (a). A higher volume of microporosity was calculated for the in vivo compared to the on shelf specimen, and pore sizes > 270 µm was only observed in the in vivo specimen. Reconstructed volumes in 3D ($2 \times 4 \times 3$ mm) for each specimen type (b).

Apart from bone formation at the interface, bone was detected in other locations, and frequently on the implant side towards the dura. Similar observations of ossification in connection to the dura have previously been made in a pre-clinical study on the same CaP–Ti combination [20], and in a clinical study on autologous bone [25]. The CaP tiles lost volume mainly on the outer side, toward the scalp, which also was seen in the µCT and histology of the retrieval specimen. The µCT and histology revealed that, toward the dura, the CaP tiles either appeared to remain intact or had started to remodel into bone. It is likely that the degradation during the first year was caused by an initial dissolution, in combination with a tribological effect between the scalp and the tiles, whereas the degradation in the remodeling process might also be cell-mediated – most likely macrophages-mediated [20,54].

The relative HU measurements showed an increase in 9 out of 10 subjects in $ROI_{implant}$. The increase was larger toward the bone defect edge, especially at the 1-year follow-up. The increase in relative HU indicates an increase in apparent density. The change in relative HU was determined in the segmented volume (implant and bone) from the last time-point, so that the CaP degradation toward the scalp did not affect the measurement. However, this led to areas were bone had formed in the last time-point being included in the first time-point, although they were then empty, and consequently the average HU-value in these areas was affected not only by changes in density but also in volume. Therefore, the apparent density increase at the interface (ROI_4) can most likely be explained by osseous bridging at the defect edge–implant interface. Nevertheless, an apparent density increase was also observed in ROI_2 and ROI_3, more clearly than in ROI_1 (central region). In these regions an overall volume loss was often observed. A general CaP degradation was observed in the retrieval specimen, which was confirmed by an increase in porosity for the CaP material (Fig. 6). Bone formation was observed between the tiles, on the edges of the tiles and also within the porosity of the tiles in this specimen (Fig. 7). In the CT images of this subject, an increase in relative HU values could be observed before implant retrieval. The increase in relative HU for most other subjects could therefore indicate similar bone formation. Korhonen et al. (2018) used similar

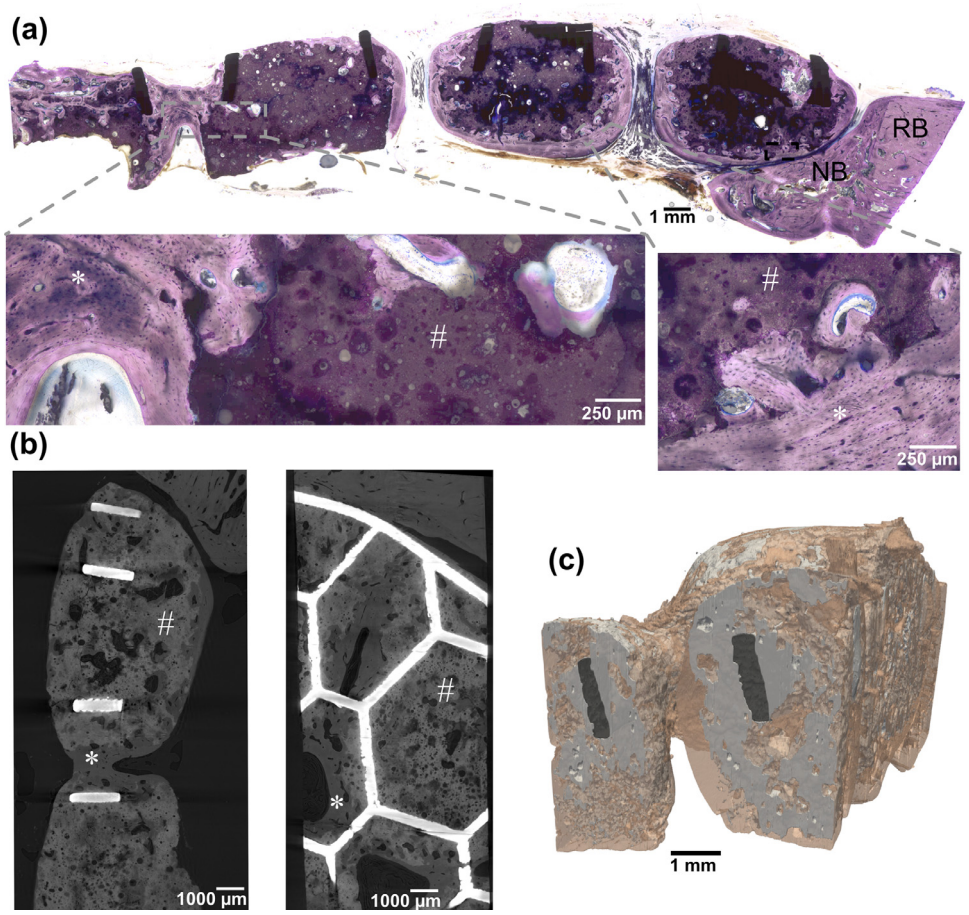

Fig. 7. Bone formation and CaP degradation in the 31-months retrieval specimen. One of the histology sections (a) with magnifications at areas of bone remodeling. The same part, and a closely neighbooring cross-section, of the specimen in the SR-µCT (b). In the SR-µCT, the specimen is also shown from the top. The newly formed (NB) as well as the recipient (RB) bone is marked in the histology. Newly formed bone (*) and remaining CaP (#) are marked in both the histology and the SR-µCT images. A 3D-model of the SR-µCT images are presented in (c), showing bone (orange), CaP (light gray) and titanium (dark gray).

methods to evaluate autologous bone resorption in cranial reconstructions [25]. Nevertheless, HU-values in clinical images have not been widely used for evaluating CaP degradation and bone remodeling and this method should be validated in future studies.

In this study, the implant sizes ranged from 25 cm^2 to 205 cm^2. These cranial defects would take several years to bridge with normal bone formation. Based on previous pre-clinical and clinical studies, the use of pure monetite in this application could lead to an excessively high degradation rate [15,55]. During preclinical studies in the development phase of the CaP–Ti implant, it was noted that the presence of β-CPP retarded the degradation rate [17,21]. Another study, which investigated brushite cement with and without the addition of pyrophosphate, found increased bone formation when using pyrophosphate [56]. That study suggested that pyrophosphate delays the conversion of brushite into the more stable HA phase, and stimulates bone formation. Moreover, β-CPP has shown a slower cell-mediated resorption in vitro, in comparison to other CaPs [57]. Future studies on the β-CPP containing monetite formulation would be of high interest for explaining this mechanism. In the studied CaP formulation, monetite was the dominant phase (85%) pre-implantation. The phase composition was different after 31 months in vivo, but monetite was still the dominating phase. Being the most soluble phase, the monetite amount decreased in vivo (to 72%). This caused an increase in the relative amount of β-TCP (from 9% to 14%), while β-CPP remained in the same amount (6%). In addition, an in vivo transformation into HA (6%), and its in vivo precursor OCP (2%), was observed. The transformation to HA, the most stable calcium orthophosphate at physiological pH, could explain the lower amount of degradation or remodeling in some CaP tiles as well as the decreased degradation rate at longer follow-ups. The observed phase transformations would be expected after extended exposure in vivo [58,59]. The same CaP formulation has previously been studied in vitro, and no phase transformations were observed after four weeks incubation in cell-media [54]. In future studies, it would be interesting to compare the phase composition from longer in vitro studies to those reported from clinical in vivo studies. This would be an important comparison that could lead to a better understanding of how in vitro conditions can simulate in vivo conditions for CaP material.

Omar et al. (2020) recently studied bone regeneration for the same monetite-based CaP formulation in ovine animal models [19]. Samples were implanted at skeletal (skull) and non-skeletal (subcutaneous) sites for 12 and 3 months, respectively. One clinical 21-months retrieval implant was also analyzed. Morphological, ultrastructural, and compositional analyses were conducted by histology, electron microscopy, and Raman spectroscopy. Bone formation was demonstrated at both skeletal and non-skeletal sites. Ultrastructural union between new bone and the CaP material was observed, and the bone was compositionally similar to native bone. Notably, the CaP material induced bone formation also at the subcutaneous site [19]. Bone was more frequently detected in the central part of the implant – which is typical for osteoinduction [60]. After in vivo exposure, Omar et al. (2020) detected a phase com-

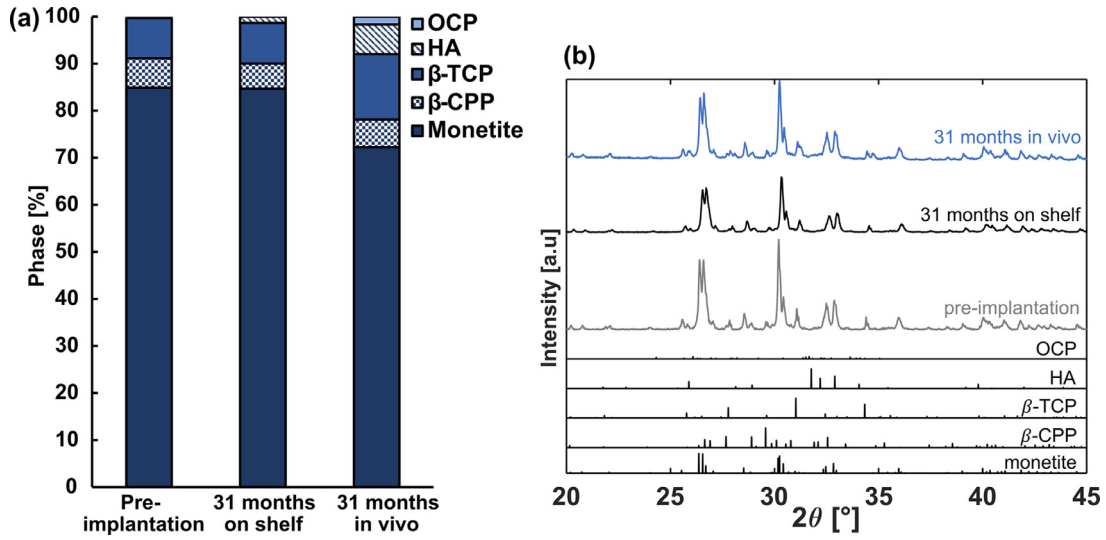

Fig. 8. Results from the XRD phase composition analysis. The relative phase composition from the Rietveld refinement (a) are presented pre-implantation, after 31 months on shelf and after 31 months in vivo. Two XRD patterns are shown for reference for samples from the analysis after 31 months on shelf and after 31 months in vivo (b).

position in the retrieval implant of 69.5% calcium deficient HA, 15% magnesium substituted TCP, 6.3% β-TCP, 6.5% β-CPP and 2.6% monetite. The reason why this differs from the XRD results in the present study is likely that they analyzed a part of the implant that was well integrated in the bone, while this study analyzed a part of the implant that fell off during retrieval surgery – the brittle behavior indicating that it was not well integrated with the bone. Hence, the found phase composition is likely not representative of the full implant due to the limited amount of sample. Nevertheless, the main purpose of the XRD analysis in the present study was to compare phase composition changes after implantation and storage of the same material, and not to indicate bone formation since this was evaluated through other analyses.

To the authors' knowledge, the present study is the first to carry out longitudinal quantifications of volume and density across a whole CaP implant site in patients. The methods developed in this study allowed for longitudinal measurements in spatially different locations of the cranial implants. Limitations of this method are related to the lack of contrast between the bone and CaP in the clinical CT images due to their similar X-ray attenuation and the relatively low CT resolution. It is clear that the volumetric reductions of the CaP tiles are CaP degradation, and that the volumetric increase is bone formation. Remodeling of CaP into bone was observed in the histology and µCT, but could not be revealed in the clinical CT images.

Several parameters are important in quantitative analysis of CT image data: standardizing the scanner and data acquisition settings, minimizing image artifacts, selecting an appropriate reconstruction algorithm, and maximizing repeatability and objectivity during the analysis [23]. As this study was made retrospectively, the settings for acquiring the CT images were not controlled. Nevertheless, the same scanner, similar resolution and the same reconstruction methods were used for the postoperative and 1-year postoperative datasets. There were differences in the scanning acquisition parameters with regard to voltage (100 or 120 kVp) and slice thickness (0.625 mm or 1.25 mm) for some scans. There was more spread in acquisition parameters at the later follow-ups, which could explain why three such CT datasets were excluded at the validation step. A fully automatic analysis of the images was not possible due to differences in the sizes and shapes of the implants. However, the quantitative analysis was conducted as repeatable and objective as possible by keeping segmentation and construction of the analyzed regions (ROIs) to semiautomatic methods. All CT-images have an inherent limit in the resolution, if a voxel contain several tissues the HU-value will be averaged. This effect is commonly referred to as the partial volume effect. A thorough analysis of the measurement errors caused by the above mentioned issues was not possible, as it would have required phantoms of a known similar volume of the analyzed implant (and bone) scanned with all the used settings. However, several measures were taken in order to ensure and demonstrate that the measurements were of high quality. The validation step made on $ROI_{control}$ confirmed that the image quality did not change between time-points in a way that affected relative volumetric measurements (scans with >3% difference were excluded). A high spatial overlap of volumes in between time-points in $ROI_{control}$ was demonstrated by measurements of DSCs and HDs. Moreover, the measured thickness of the tiles in the retrieval specimen µCT was similar as compared to the clinical CT, 5.7 ± 0.5 mm vs. 5.8 ± 0.6 mm. The relative change in volume and density in relation to the baseline CT was always reported, instead of absolute values. Relative measurements were more situatable since no calibration with phantoms were made. A baseline CT was always included so that measurements of relative changes could be performed instead of absolute values. Lastly, intrasubject calibration was used for the HU-values [25,38].

A limitation of this study was the low number of subjects. Future studies should increase both the number of subjects and the number of time-points for each subject. The present study identified time-points of interest. Early CaP degradation would be of great interest to analyze in three to six months postoperative CT scans. Furthermore, longer follow-ups would be necessary to investigate whether the volumetric balance is kept and if the bone formation continues, e.g. if the gaps between the tiles would close on the long term. The relatively low number of subjects included in the present study did not allow for any statistical analysis with respect to patient demographics. In relation to CaP degradation and bone regeneration, it would be of interest to analyze e.g. age or impact of radiation therapy. Moreover, the position of the defect might affect the result since a superior healing capacity in the frontal bone as compared to parietal/temporal bones has previously been identified [10,61], and would be of interest to further investigate. Finally, it is not known how bone regeneration and CaP degradation affect the mechanical properties of CaPs. These

mechanical properties could be investigated through longitudinal quantitative data on bone formation and CaP degradation in combination with computational models (e.g. [62]).

5. Conclusions

This is the first study that quantitatively measures longitudinal volumes of monetite-based CaPs in an entire clinical implant site. One year after implantation, the volume of the CaP–Ti implant had decreased due to CaP degradation, but the change plateaued at the 3-year follow-up. Bone formation, as detected by an increased volume, was seen at the implant–bone interface of all subjects. The results of this study show a long-term volumetric balance and osteoconduction in cranial defects with the CaP–Ti implant, which is of great importance for successful clinical results in larger defects. The present study makes methodological advancements in clinical quantitative assessment of calcium phosphate materials. The developed methods could be used in future studies for correlating bone regeneration and CaP degradation with patient demographics and implant site location.

Declaration of Competing Interest

Dr. Lewin, Prof. Persson and Assoc.Prof. Öhman-Mägi have no interests to declare. Dr. Gallinetti and Dr. Birgersson report personal fees from OssDsign both during the conduct of the study and outside the submitted work. Dr. Åberg, Dr. Kihlström Burenstam Linder and Prof. Engqvist have consulting agreements with OssDsign. Dr. Åberg and Prof. Engqvist have direct ownership in OssDsign, and Prof. Engqvist is on the board of OssDsign.

Acknowledgements

Funding from the Eurostars-2 Joint European Union's Horizon 2020 (project ID: E19741) is acknowledged. The acknowledgement is extended to the Paul Scherrer Institut, Villigen, Switzerland for TOMCAT beamtime, and to Federica Marone, Per Isaksson, Jenny Carlsson, Dan Wu and Magnus Heldin for their assistance during the experiments at PSI.

Supplementary materials

Supplementary material associated with this article can be found, in the online version, at doi:10.1016/j.actbio.2021.04.015.

References

[1] W. Habraken, P. Habibovic, M. Epple, M. Bohner, Calcium phosphates in biomedical applications: materials for the future? Mater. Today 19 (2016) 69–87, doi:10.1016/j.mattod.2015.10.008.
[2] S.E.C.M. van de Vijfeijken, T.J.A.G. Münker, R. Spijker, L.H.E. Karssemakers, W.P. Vandertop, A.G. Becking, D.T. Ubbink, Autologous Bone Is Inferior to Alloplastic Cranioplasties: safety of Autograft and Allograft Materials for Cranioplasties, a Systematic Review, World Neurosurg. 117 (2018) 443–452 .e8, doi:10.1016/j.wneu.2018.05.193.
[3] E. Neovius, T. Engstrand, Craniofacial reconstruction with bone and biomaterials: review over the last 11 years, J. Plastic Reconstr. Aesthetic Surg. 63 (2010) 1615–1623, doi:10.1016/j.bjps.2009.06.003.
[4] T. Engstrand, L. Kihlström Burenstam Linder, E. Neovius, A.-C.D. Skogh, T.K. Lundgren, H. Jacobsson, J. Bohlin, J. Åberg, H. Engqvist, Development of a bioactive implant for repair and potential healing of cranial defects, J. Neurosurg. 120 (2014) 273–277.
[5] R. Stefini, G. Esposito, B. Zanotti, C. Iaccarino, M.M. Fontanella, F. Servadei, Use of "custom made" porous hydroxyapatite implants for cranioplasty: postoperative analysis of complications in 1549 patients, Surg. Neurol. Int. 4 (2013).
[6] K.M.J. Aitasalo, J.M. Piitulainen, J. Rekola, P.K. Vallittu, Craniofacial bone reconstruction with bioactive fiber-reinforced composite implant, Head Neck 36 (2014) 722–728, doi:10.1002/hed.23370.
[7] J. Brie, T. Chartier, C. Chaput, C. Delage, B. Pradeau, F. Caire, M.-P. Boncoeur, J.-J. Moreau, A new custom made bioceramic implant for the repair of large and complex craniofacial bone defects, J. Cranio-Maxillofacial Surg. 41 (2013) 403–407, doi:10.1016/j.jcms.2012.11.005.
[8] J.M. Piitulainen, J.P. Posti, P.K. Vallittu, K.M. Aitasalo, W. Serlo, A Large Calvarial Bone Defect in a Child: osseointegration of an Implant, World Neurosurg. 124 (2019) 282–286, doi:10.1016/j.wneu.2019.01.028.
[9] P.K. Vallittu, J.P. Posti, J.M. Piitulainen, W. Serlo, J.A. Määttä, T.J. Heino, S. Pagliari, S.M. Syrjänen, G. Forte, Biomaterial and implant induced ossification: in vitro and in vivo findings, J. Tissue Eng. Regen. Med. 14 (2020) 1157–1168, doi:10.1002/term.3056.
[10] A.-C.D. Skogh, L. Kihlström Burenstam Linder, E. Neovius, C. Persson, M.O. Beckman, T. Engstrand, Variation in Calvarial Bone Healing Capacity: a Clinical Study on the Effects of BMP-2-Hydrogel or Bone Autograft Treatments at Different Cranial Locations, J. Craniofac. Surg. 24 (2013) 339–343, doi:10.1097/SCS.0b013e31827ff2b6.
[11] E. Kohan, J. Roostaeian, J.T. Yuan, K.L. Fan, C. Federico, H. Kawamoto, J.P. Bradley, Customized bilaminar resorbable mesh with BMP-2 promotes cranial bone defect healing, Ann Plast Surg 74 (2015) 603–608, doi:10.1097/01.sap.0000465206.62522.af.
[12] J. Lu, M. Descamps, J. Dejou, G. Koubi, P. Hardouin, J. Lemaitre, J.-P. Proust, The biodegradation mechanism of calcium phosphate biomaterials in bone, J. Biomed. Mater. Res. 63 (2002) 408–412, doi:10.1002/jbm.10259.
[13] F. Tamimi, Z. Sheikh, J. Barralet, Dicalcium phosphate cements: brushite and monetite, Acta Biomater. 8 (2012) 474–487.
[14] L. Schröter, F. Kaiser, S. Stein, U. Gbureck, A. Ignatius, Biological and mechanical performance and degradation characteristics of calcium phosphate cements in large animals and humans, Acta Biomater. 117 (2020) 1–20, doi:10.1016/j.actbio.2020.09.031.
[15] F. Tamimi, J. Torres, D. Bassett, J. Barralet, E.L. Cabarcos, Resorption of monetite granules in alveolar bone defects in human patients, Biomaterials 31 (2010) 2762–2769.
[16] L.Kihlström Burenstam Linder, U. Birgersson, K. Lundgren, C. Illies, T. Engstrand, Patient-Specific Titanium-Reinforced Calcium Phosphate Implant for the Repair and Healing of Complex Cranial Defects, World Neurosurg. (2018), doi:10.1016/j.wneu.2018.10.061.
[17] T. Engstrand, L. Kihlström Burenstam Linder, K. Lundgren, M. Trobos, H. Engqvist, P. Thomsen, Bioceramic Implant Induces Bone Healing of Cranial Defects, Plast Reconstr. Surg. Glob. Open 3 (2015), doi:10.1097/GOX.0000000000000467.
[18] J. Sundblom, D. Nowinski, O. Casar-Borota, M. Ryttlefors, Removal of giant intraosseous meningioma followed by cranioplasty using a custom-made bioceramic implant: case report, J. Neurosurg. (2018) 1–5, doi:10.3171/2018.4.JNS1850.
[19] O. Omar, T. Engstrand, L. Kihlström Burenstam Linder, J. Åberg, F.A. Shah, A. Palmquist, U. Birgersson, I. Elgali, M. Pujari-Palmer, H. Engqvist, P. Thomsen, In situ bone regeneration of large cranial defects using synthetic ceramic implants with a tailored composition and design, Proc. Natl. Acad. Sci. 117 (2020) 26660–26671, doi:10.1073/pnas.2007635117.
[20] S. Gallinetti, L. Kihlström Burenstam Linder, J. Åberg, C. Illies, H. Engqvist, U. Birgersson, Titanium reinforced calcium phosphate improves bone formation and osteointegration in ovine calvaria defects: a comparative 52-weeks study, Biomed. Mater. (2020), doi:10.1088/1748-605X/abca12.
[21] J. Åberg, T. Engstrand, H. Engqvist, Cement-forming compositions, monetite cements, implants and methods for correcting bone defects, Google Patents (2018).
[22] S. Lewin, J. Åberg, D. Neuhaus, H. Engqvist, S.J. Ferguson, C. Öhman-Mägi, B. Helgason, C. Persson, Mechanical behaviour of composite calcium phosphate–titanium cranial implants: effects of loading rate and design, J. Mech. Behav. Biomed. Mater. 104 (2020) 103701, doi:10.1016/j.jmbbm.2020.103701.
[23] K.L. Troy, W.B. Edwards, Practical considerations for obtaining high quality quantitative computed tomography data of the skeletal system, Bone (2018), doi:10.1016/j.bone.2018.01.013.
[24] W.A. Kalender, Computed Tomography: Fundamentals, System Technology, Image Quality, Applications, John Wiley & Sons, 2011.
[25] T.K. Korhonen, N. Salokorpi, J. Niinimäki, W. Serlo, P. Lehenkari, S. Tetri, Quantitative and qualitative analysis of bone flap resorption in patients undergoing cranioplasty after decompressive craniectomy, J. Neurosurg. 130 (2018) 312–321, doi:10.3171/2017.8.JNS171857.
[26] L.R. Barzaghi, V. Parisi, C.R. Gigliotti, L. Giudice, S. Snider, A. Dell'Acqua, A. del Vecchio, P. Mortini, Bone resorption in autologous cryopreserved cranioplasty: quantitative evaluation, semiquantitative score and clinical significance, Acta Neurochir. (Wien) 161 (2019) 483–491.
[27] A. Moles, P.M. Heudes, A. Amelot, J. Cristini, C. Salaud, V. Roualdes, T. Riem, S.A. Martin, S. Raoul, L. Terreaux, E. Bord, K. Buffenoir, Long-Term Follow-Up Comparative Study of Hydroxyapatite and Autologous Cranioplasties: complications, Cosmetic Results, Osseointegration, World Neurosurg. 111 (2018) e395–e402, doi:10.1016/j.wneu.2017.12.082.
[28] L. Zaccaria, S.J. Tharakan, S. Altermatt, Hydroxyapatite ceramic implants for cranioplasty in children: a single-center experience, Childs Nerv. Syst. 33 (2017) 343–348, doi:10.1007/s00381-016-3327-4.
[29] W. Maenhoudt, G. Hallaert, J.-P. Kalala, E. Baert, F. Dewaele, W. Bauters, D. Van Roost, Hydroxyapatite cranioplasty: a retrospective evaluation of osteointegration in 17 cases, Acta Neurochir. (Wien) 160 (2018) 2117–2124.
[30] P. Christen, K. Ito, R. Ellouz, S. Boutroy, E. Sornay-Rendu, R.D. Chapurlat, B. Van Rietbergen, Bone remodelling in humans is load-driven but not lazy, Nat. Commun. 5 (2014) 4855, doi:10.1038/ncomms5855.

[31] A. Fedorov, R. Beichel, J. Kalpathy-Cramer, J. Finet, J.-C. Fillion-Robin, S. Pujol, C. Bauer, D. Jennings, F. Fennessy, M. Sonka, J. Buatti, S. Aylward, J.V. Miller, S. Pieper, R. Kikinis, 3D Slicer as an image computing platform for the Quantitative Imaging Network, Magn. Reson. Imaging 30 (2012) 1323–1341, doi:10.1016/j.mri.2012.05.001.
[32] N. Otsu, A Threshold Selection Method from Gray-Level Histograms, IEEE Trans. Syst. Man Cybern. 9 (1979) 62–66, doi:10.1109/TSMC.1979.4310076.
[33] S. Lewin, C. Riben, A. Thor, C. Öhman-Mägi, Bone Volume Assessment Around Dental Implants After Open Maxillary Sinus Elevation Surgery: A Quantitative Approach to CBCT Images, Int. J. Oral Maxillofacial Implants 34 (2) (2019) 489–498, doi:10.11607/jomi.7150.
[34] D.P. Huttenlocher, G.A. Klanderman, W.J. Rucklidge, Comparing images using the Hausdorff distance, IEEE Trans. Pattern Anal. Mach. Intell. 15 (1993) 850–863, doi:10.1109/34.232073.
[35] L.R. Dice, Measures of the amount of ecologic association between species, Ecology 26 (1945) 297–302.
[36] C. Levi, J.E. Gray, E.C. McCullough, R.R. Hattery, The unreliability of CT numbers as absolute values, Am. J. Roentgenol. 139 (1982) 443–447.
[37] B.A. Birnbaum, N. Hindman, J. Lee, J.S. Babb, Multi–detector row CT attenuation measurements: assessment of intra-and interscanner variability with an anthropomorphic body CT phantom, Radiology 242 (2007) 109–119.
[38] M.F. Boomsma, I. Slouwerhof, J.A. van Dalen, M.A. Edens, D. Mueller, J. Milles, M. Maas, Use of internal references for assessing CT density measurements of the pelvis as replacement for use of an external phantom, Skeletal Radiol. 44 (2015) 1597–1602, doi:10.1007/s00256-015-2206-5.
[39] D. Paganin, S.C. Mayo, T.E. Gureyev, P.R. Miller, S.W. Wilkins, Simultaneous phase and amplitude extraction from a single defocused image of a homogeneous object, J. Microsc. 206 (2002) 33–40, doi:10.1046/j.1365-2818.2002.01010.x.
[40] A. Groso, R. Abela, M. Stampanoni, Implementation of a fast method for high resolution phase contrast tomography, Opt. Express, OE. 14 (2006) 8103–8110, doi:10.1364/OE.14.008103.
[41] F. Marone, M. Stampanoni, Regridding reconstruction algorithm for real-time tomographic imaging, J. Synchrotron. Rad. 19 (2012) 1029–1037, doi:10.1107/S0909049512032864.
[42] J. Schindelin, I. Arganda-Carreras, E. Frise, V. Kaynig, M. Longair, T. Pietzsch, S. Preibisch, C. Rueden, S. Saalfeld, B. Schmid, Fiji: an open-source platform for biological-image analysis, Nat. Methods 9 (2012) 676–682.
[43] S. Lewin, A. Barba, C. Persson, J. Franch, M.-.P. Ginebra, C. Öhman-Mägi, Evaluation of bone formation in calcium phosphate scaffolds with μ CT-method validation using SEM, Biomed. Mater. 12 (2017) 065005, doi:10.1088/1748-605X/aa801d.
[44] J. Bergmann, P. Friedel, R. Kleeberg, BGMN–a new fundamental parameters based Rietveld program for laboratory X-ray sources; it's use in quantitative analysis and structure investigations, (1998).
[45] N. Doebelin, R. Kleeberg, Profex: a graphical user interface for the Rietveld refinement program BGMN, J. Appl. Crystallogr. 48 (2015) 1573–1580.
[46] B. Dickens, L.W. Schroeder, W.E. Brown, Crystallographic studies of the role of Mg as a stabilizing impurity in β-Ca3 (PO4) 2. The crystal structure of pure β-Ca3 (PO4) 2, J. Solid State Chem. 10 (1974) 232–248.
[47] N.A. Curry, D.W. Jones, Crystal structure of brushite, calcium hydrogen orthophosphate dihydrate: a neutron-diffraction investigation, J. Chem. Soc. A (1971) 3725–3729.
[48] S. Boudin, A. Grandin, M.M. Borel, A. Leclaire, B. Raveau, Redetermination of the β-Ca2P2O7 structure, Acta Crystallogr. Sect. C 49 (1993) 2062–2064.
[49] B. Dickens, J.S. Bowen, W.E. Brown, A refinement of the crystal structure of CaHPO4 (synthetic monetite), Acta Crystallographica Section B: Struct. Crystallogr. Crystal Chem. 28 (1972) 797–806.
[50] K.T. Sudarsanan, R.A. Young, Significant precision in crystal structural details. Holly Springs hydroxyapatite, Acta Crystallographica Section B: Struct. Crystallogr. Crystal Chem. 25 (1969) 1534–1543.
[51] M. Mathew, W.E. Brown, L.W. Schroeder, B. Dickens, Crystal structure of octacalcium bis (hydrogenphosphate) tetrakis (phosphate) pentahydrate, Ca 8 (HP0 4) 2 (PO 4) 4• 5H 2 O, J. Crystallogr. Spectrosc. Res. 18 (1988) 235–250.
[52] R Core TeamR: A language and Environment For Statistical Computing, R Foundation for Statistical Computing, Vienna, Austria, 2014 URL http://www.R-project.org/ .
[53] T. Engstrand, Biomaterials and biologics in craniofacial reconstruction, J. Craniofac. Surg. 23 (2012) 239–242.
[54] M. Montazerolghaem, M. Karlsson Ott, H. Engqvist, H. Melhus, A.J. Rasmusson, Resorption of monetite calcium phosphate cement by mouse bone marrow derived osteoclasts, Mater. Sci. Eng. C 52 (2015) 212–218, doi:10.1016/j.msec.2015.03.038.
[55] Z. Sheikh, Y.L. Zhang, L. Grover, G.E. Merle, F. Tamimi, J. Barralet, In vitro degradation and in vivo resorption of dicalcium phosphate cement based grafts, Acta Biomater. 26 (2015) 338–346.
[56] L.M. Grover, A.J. Wright, U. Gbureck, A. Bolarinwa, J. Song, Y. Liu, D.F. Farrar, G. Howling, J. Rose, J.E. Barralet, The effect of amorphous pyrophosphate on calcium phosphate cement resorption and bone generation, Biomaterials 34 (2013) 6631–6637, doi:10.1016/j.biomaterials.2013.05.001.
[57] V.M. Wu, V. Uskoković, Is there a relationship between solubility and resorbability of different calcium phosphate phases in vitro? Biochimica et Biophysica Acta (BBA)-General Subjects 1860 (2016) 2157–2168.
[58] F. Tamimi, D.L. Nihouannen, H. Eimar, Z. Sheikh, S. Komarova, J. Barralet, The effect of autoclaving on the physical and biological properties of dicalcium phosphate dihydrate bioceramics: brushite vs. monetite, Acta Biomater. 8 (2012) 3161–3169, doi:10.1016/j.actbio.2012.04.025.
[59] A. Bannerman, R.L. Williams, S.C. Cox, L.M. Grover, Visualising phase change in a brushite-based calcium phosphate ceramic, Sci. Rep. 6 (2016) 1–10, doi:10.1038/srep32671.
[60] M. Bohner, R.J. Miron, A proposed mechanism for material-induced heterotopic ossification, Mater. Today 22 (2019) 132–141, doi:10.1016/j.mattod.2018.10.036.
[61] D. Lo, A. McArdle, K. Senarath-Yapa, M. Longaker, Commentary on the differential healing capacity of calvarial bone, J Craniofac Surg 24 (2013) 344–345, doi:10.1097/SCS.0b013e3182802256.
[62] S. Lewin, I. Fleps, D. Neuhaus, C. Öhman-Mägi, S.J. Ferguson, C. Persson, B. Helgason, Implicit and explicit finite element models predict the mechanical response of calcium phosphate-titanium cranial implants, J. Mech. Behav. Biomed. Mater. (2020) 104085, doi:10.1016/j.jmbbm.2020.104085.